Size dependent hygroscopicity of levoglucosan and D-glucose aerosol nanoparticles

Ting Lei[1,2], Hang Su[2,3], Nan Ma[4], Ulrich Pöschl[2], Alfred Wiedensohler[5], Yafang Cheng[1]

[1]Minerva Research Group, Max Planck Institute for Chemistry, 55128 Mainz, Germany

[2]Multiphase Chemistry Department, Max Planck Institute for Chemistry, 55128 Mainz, Germany

[3]State Environmental Protection Key Laboratory of Formation and Prevention of Urban Air Pollution Complex, Shanghai Academy of Environmental Sciences, Shanghai 200233, China

[4]Institute for Environmental and Climate Research, Jinan University, 511443 Guangzhou, China

[5]Leibniz Institute for Tropospheric Research, 04318 Leipzig, Germany

Correspondence to: Yafang Cheng (yafang.cheng@mpic.de)

Abstract: The interaction between water vapor and aerosol nanoparticles is important in atmospheric processes. Hygroscopicity of sub-10 nm organic nanoparticles and their concentration-dependent thermodynamic properties (e.g., water activity) in the highly supersaturated concentration range are, however, scarcely available. Here we investigate the size dependence of hygroscopicity of organics (i.e., levoglucosan, D-glucose) in dry particle diameter down to 6 nm using a nano-hygroscopicity tandem differential mobility analyzer (nano-HTDMA). Our results show that there is only a weak size dependent hygroscopic growth of both levoglucosan and D-glucose nanoparticles with diameters down to 20 nm. In the diameter range smaller than 20 nm (down to 6 nm), we observed a strong size-dependent hygroscopic growth for D-glucose nanoparticles. The hygroscopic growth factors cannot be determined for levoglucosan below 20

nm due to its evaporation. In addition, we compare hygroscopicity measurements for levoglucosan and D-glucose nanoparticles with the E-AIM (standard UNIFAC), the ideal solution theory, and DKA predictions, respectively. The ideal solution theory describes well the measured hygroscopic growth factors of levoglucosan with diameters down to 20 nm and D-glucose nanoparticles with diameters higher than 60 nm, respectively, while the E-AIM (standard UNIFAC) model can successfully predict the growth factors of D-glucose nanoparticles with diameters from 100 down to 6 nm at RH above 88-40 % (e.g., at RH above 88 % for 100 nm D-glucose, at RH above 40 % for 6 nm D-glucose). The use of the DKA method leads to a good agreement with measured hygroscopic growth factors of D-glucose aerosol nanoparticles with diameters from 100 down to 6 nm. Predicted water activity for these aqueous organic solutions (i.e., levoglucosan, D-glucose) from different parameterization methods agrees well with observations in the low solute concentration range (< 20 mol kg^{-1}), and start to deviate from observations in the high solute concentration (> 20 mol kg^{-1}).

1 Introduction

Organic aerosol nanoparticles play an important role in new particle formation, subsequent condensation and coagulation growth, cloud condensation nuclei (CCN), and thus in affecting visibility degradation, radiative forcing, and climate (Chylek and Coakley, 1974; Charlson et al., 1992; Dusek et al., 2010; Cheng et al., 2012; Zhang et al., 2012; Kulmala et al., 2013). Both growth of nanoparticles and their ability to act as CCN are directly related to its hygroscopicity that describes the interaction between organic nanoparticles and water vapor (Köhler, 1936; Kreidenweis et al., 2005; Su et al., 2010; Cheng et al., 2015; Wang et al., 2015). However, current knowledge of hygroscopicity of sub-10 nm organic nanoparticles and their concentration-

dependent thermodynamic properties (e.g., water activity) in the highly supersaturated concentration range is scarcely available.

Levoglucosan aerosol nanoparticles have attracted increasing interest in recent years (Simoneit et al., 1999; Mochida and Kawamura, 2004; Mikhailov et al., 2009; Elias et al., 2010; Lei et al., 2014, 2018; Bhattarai et al., 2019) and is considered as an ideal tracer for characterization and quantification of the biomass burning (Fraser and Lakshmanan, 2000). Also, levoglucosan is typically the most abundant species in wood burning aerosols, which contributes substantially (16.6–30.9% by mass) to the total organics in PM2.5 (Mochida and Kawamura, 2004; Bhattarai et al., 2019). D-glucose, a hydrolysis product of cellulose and levoglucosan, is a major pyrolysis product of wood (Mochida and Kawamura, 2004; Bhattarai et al., 2019; Mikhailov and Vlasenko., 2020). Hygroscopicity of levoglucosan and D-glucose substances is thus important in reproducing the overall hygroscopic behavior of the real biomass burning aerosol particles (Bhandari and Bareyre. 2003; Mochida and Kawamura, 2004; Chan et al., 2005; Koehler et al., 2006; Peng et al., 2010; Mikhailov and Vlasenko., 2020). For example, a small difference in the hygroscopicity parameter (κ) is observed between measured data of model mixtures including levoglucosan and ammonium sulfate in the laboratory using the hygroscopicity tandem differential mobility analyzer (HTDMA) and biomass burning aerosol particles in the field using CCN activity measurement due to the similar O: C ratios of levoglucosan and ammonium sulfate mass fractions used in model mixtures when experimental κ data from sub- and supersaturated water vapor conditions are compared (Bhandari and Bareyre. 2003; Mochida and Kawamura, 2004; Chan et al., 2005; Koehler et al., 2006; Peng et al., 2010; Pöhlker et al., 2016; Lei et al., 2018; Mikhailov and Vlasenko., 2020). Most of the previous lab studies have focused on investigation of the hygroscopic behavior of 100-nm levoglucosan and D-glucose aerosol nanoparticles, which mainly utilized the humidified

tandem differential mobility analyzers (DMAs) (Mikhailov et al., 2004; Mochida and Kawamura. 2004; Koehler et al., 2006; Lei et al., 2014; 2018). For example, Mochida and Kawamura (2004) observed that 100-nm levoglucosan and D-glucose aerosol nanoparticles uptake/release water continuously in both deliquescence and efflorescence modes, respectively. To our knowledge, there are no phase transitions for these organic aerosol nanoparticles in both deliquescence and efflorescence processes.

Early studies showed that the hygroscopicity and solubility of inorganic aerosols, such as ammonium sulfate (AS) and sodium chloride (NaCl), exhibited a strong size dependence (Cheng et al., 2015). Firstly, hygroscopic diameter growth factors of AS, NaCl as well as Na_2SO_4 nanoparticles are found to decrease with size decreases in both deliquescence and efflorescence modes (Biskos et al., 2006a, b, c, Lei et al., 2020). Secondly, there is no significant difference in the deliquescence relative humidity (DRH) and the efflorescence relative humidity (ERH) between AS nanoparticles with dry diameters of 6 and 60 nm (Biskos et al., 2006b; Lei et al., 2020), while a pronounced size dependence of the DRH of NaCl is up to 10 % RH between dry diameters of 6 and 60 nm (Biskos et al., 2006a). The behaviors of change of phase transition RH and concentrations of Na_2SO_4 are between NaCl and AS (Lei et al., 2020). However, there are very few lab studies on investigating hygroscopicity (g_f, DRH, ERH) of organic aerosol nanoparticles in sub-10 nm size range (Wang et al., 2017). It is not clear how the size effect influences the hygroscopic growth of organics, especially those without DRH and ERH. Besides technique limitation (Lei et al., 2020; Wang et al., 2017), another reason is the high diffusion of sub-100 nm organic nanoparticles, especially in the sub-10 nm size range, which results in nanoparticle losses in the HTDMA system (Seinfeld and Pandis, 2006).

Thermodynamic model is widely used to predict the hygroscopic growth factor of organic aerosol particles as a function of RH (Bhandari and Bareyre. 2003; Chan et al., 2005; Koehler et al., 2006; Peng et al., 2010). The current thermodynamic models mainly rely on the concentration-dependent thermodynamic data (such as water activity, liquid-vapor interfacial energy), which are often derived from the measurements of large droplets and/or bulk solution (Tang and Munkelwitz, 1994; Tang 1996; Pruppacher and Klett, 1997; Clegg et al., 1998). Nanodroplets can become more highly supersaturated and thus reaching higher solute concentration compared to bulk solution, which makes it difficult for models to predict its hygroscopicity. Cheng et al. (2015) pointed out that size effect might be taken models into account. By measuring the hygroscopic growth factor of organic nanoparticles (e.g., levoglucosan and D-glucose) of different sizes, we may be able to retrieve these thermodynamic data using a Differential Köhler Analysis (DKA) method (Cheng et al., 2015). This will further help us to understand of the new particle formation, transportation, and their interactions with water molecules.

In this study, we investigate the hygroscopic growth factors of levoglucosan and D-glucose nanoparticles in size down to 6 nm using a nano-hygroscopic tandem differential mobility analyzer (nano-HTDMA, Lei et al., 2020). Moreover, we compare our measurement data with model prediction from the Extended Aerosol Inorganic Model (E-AIM (standard UNIFAC)) (Clegg et al., 2001; Clegg and Seinfeld, 2006; available online: http://www.aim.env.ac.uk/aim/aim.php), the ideal solution theory, and DKA. In addition, the use of the DKA method is to calculate thermodynamic properties (e.g., water activity) of D-glucose nanodroplets in the highly supersaturated concentration range and then to compare with KD-derived data (KD=Kreidenweis), thermodynamic property data from Köhler (Kreidenweis et al., 2005), E-AIM (standard UNIFAC) model, and references, respectively.

2 Methodology

2.1 Experimental methods

2.1.1 Nanoparticle generation

An electrospray is employed to generate levoglucosan and D-glucose aerosol nanoparticles of 6, 8, 10, and 15 nm using 2, 3, 5, and 10 mM aqueous solutions with 50 % volume fraction of a 20 mM ammonium acetate buffer solution (Chen et al., 2005; Wang et al., 2015), respectively. The generated nanoparticles are diluted by mixing with dry and filtered N_2 (1 l/min) and CO_2 (0.1 l/min), bringing aerosol nanoparticles to a dry RH state ($\leq$ 2% RH). Subsequently, aerosol nanoparticles pass through a Po^{210} neutralizer to reach the equilibrium charge distribution (Wiedensohler 1986). In order to avoid blocking the 25-μm capillary tube in the electrospray with high concentration solution, the aerosol nanoparticles with diameters of 60-100 and 20 nm are generated by an atomizer with a 0.05 and 0.01 wt % organic solution (i.e., levoglucosan and D-glucose), respectively. The chemical substances and their physical properties are characterized in Table S1. These solutions are prepared with distilled and de-ionized million-Q water (resistivity of 18.2 MΩ cm at 298.15 K). Note that the size selected by the nano-DMA1 should be the right part of peak diameter of the number size distribution of the generated nanoparticles, which minimizes the influence of the multiple charged nanoparticles in hygroscopicity measurements. This is to ensure that we could have as many particles as possible to compensate for the strong loss of very small particles in the whole humidification system.

2.1.2 Nano-HTDMA setup

Figure 1 shows a schematic of the nano-HTDMA system for investigating the hygroscopic behavior of aerosol nanoparticles, especially in the sub-10 nm size range. The detailed description, calibration, and validation of nano-HTDMA setup have been reported in the previous paper (Lei et al., 2020). In brief, the polydisperse aerosol nanoparticles pass through a silica gel diffusion dryer and a Nafion gas dryer (TROPOS Model ND.070, Length 60 cm). The dry aerosol nanoparticles at RH below 10 % are charged by a Kr^{85} bipolar charger and then enter the first nano-differential mobility analyzer (nano-DMA1, TROPOS Model Vienna-type short DMA), where a monodisperse distribution of nanoparticles with the desired dry diameter is selected. The monodispersed nanoparticles subsequently are exposed to the different RH conditions, which can be set to deliquescence mode (from low RH to high RH for measuring deliquescence) or efflorescence mode (from the high RH to low RH for measuring efflorescence). In the deliquescence mode, the dry aerosol nanoparticles are gradually humidified to a target RH through a Nafion humidifier (NH-1, TROPOS Model ND.070, Length 60 cm). In the efflorescence mode, after deliquescence of aerosol nanoparticles with RH above 97% in a Nafion humidifier (NH-2: Perma Pure Model MH-110, Length 30 cm), the deliquesced aerosol nanoparticles are stepwise dried to a target RH in NH-1. The number size distribution of the humidified nanoparticles is then measured by a nano-differential mobility analyzer (nano-DMA2) at a target RH through a Nafion humidifier (NH-3, Perma Pure Model PD-100) coupled with an ultrafine condensation particle counter (CPC, TSI, model no. 3776). To have the uniform RH within the nano-DMA2 for the accurate determination of hygroscopicity (g_f, DRH, ERH) of aerosol nanoparticles, the difference between the sheath flow RH (RH_s) and the aerosol flow RH (RH_a) upstream of the nano-DMA2 is kept <1 %. Most importantly, the temperature difference between inlet and outlet of the nano-DMA2 is maintained below 0.2 °C during the measurements. In addition, the residence time (e.g., 5.4 s: between the

158 humidifier and the nano-DMA2; 0.07 s: deliquescence for aerosol nanoparticles) is sufficient for
159 water-soluble aerosol nanoparticles to equilibrate with water vapor at a given RH and to occur
160 solid-liquid phase transition (Kerminen 1997; Duplissy et al., 2005; Raoux et al., 2007),
161 respectively.

162 **2.2 Theory and modeling methods**

163 **2.2.1 Köhler theory**

164 The fractional ambient relative humidity ($\frac{RH}{100}$) over a spherical droplet in equilibrium with the
165 environment is described by Köhler equation (Köhler 1936):

166 $$\frac{RH}{100} = a_w exp\left(\frac{4\sigma_{sol}v_w}{RTG_f D_s}\right) \quad (1)$$

167 where a_w is the water activity of the solution droplet, σ_{sol} is the liquid-vapor interfacial energy of
168 solution droplet (also called surface tension), v_w is the partial molar volume of water, R is the
169 universal gas constant, T is the temperature, G_f is the diameter growth factor of aerosol particles,
170 and D_s is the dry diameter of spherical aerosol particles. The hygroscopic growth curve (G_f vs RH)
171 is estimated based on the assumptions in models or theories described in the following sections
172 (2.2.2-2.2.3).

173 **2.2.2 Water activity**

174 The expression for water activity used in the Simplified Kohler Theory (SKT) assumes the droplet
175 contains n_w moles of water and n_s moles of nonvolatile solute.

176 $$a_w = \frac{n_w}{n_w + \nu n_s} \quad (2)$$

177 v is the number of ions of solute present in solution (v=1 for organic composition). This expression
178 has been applied to the diluted solution (Kreidenweis et al., 2005; Koehler et al., 2006).

179 The following KD expression proposed by Kreidenweis et al. (2005) (KD= Kreidenweis) is to
180 present the relationship between a_w and *Gf* determined in hygroscopic growth measurements:

181 $$Gf = \left[1 + (a + b * a_w + c * a_w^2)\frac{a_w}{1-a_w}\right]^{\frac{1}{3}} \quad (3)$$

182 The coefficients a, b, and c for organic solution droplet in this study from Lei et al. (2014, 2018)
183 and Estillore et al. (2017) as shown in Table S2.

184 Differential Köhler analysis (DKA) proposed by Cheng et al. (2015) is theoretically based on
185 Köhler equation (Köhler, 1936) to determine water activity by measuring hygroscopic growth
186 factors of aerosol nanoparticles in different sizes.

187 $$a_w = \frac{s_{w1}^{\left(\frac{D_{s1}}{D_{s1}-D_{s2}}\right)}}{s_{w2}^{\left(\frac{D_{s2}}{D_{s1}-D_{s2}}\right)}} \quad (4)$$

188 where s_{w1} and s_{w2} are water saturation ratio measured at the same g_f but at the different initial dry
189 diameters (D_{s1}, D_{s2}), respectively. Using the DKA method can calculate the water activity in the
190 highly supersaturated concentration range.

191 **2.2.3 Growth factor**

192 For ideal solution, the hygroscopic curve can be estimated assuming that the water activity a_w of
193 the solution containing non-volatile and non-electrolyte solute component is equal to the molar
194 ratio of water in the solution. Here, the partial molar volume of pure water in the solution is equal
195 to the molar volume of pure water. Since the hygroscopic diameter growth factor measurements

are on volume basis using nano-HTDMA system, the expression of G_f as a function of molar ratio (x_j), molar mass (M_j), and mass density (ρ_j) of components j as follows:

$$G_f = \left[\frac{\sum_j \left(x_j M_j \frac{1}{\rho_j}\right)}{\sum_{j,j\neq w}\left(x_j M_j \frac{1}{\rho_j}\right)}\right]^{\frac{1}{3}} \quad (5)$$

The hygroscopic growth curve of aerosol particles is commonly evaluated from Extend-Aerosol Inorganic Model (E-AIM). It is a thermodynamic equilibrium model used for calculating phase partitioning (gas/liquid/solid). Most importantly, the E-AIM mode can model thermodynamic properties (e.g., water activity, liquid-vapor interfacial energy, and solution density) in the highly supersaturated concentration solution (Dutcher et al., 2013). Also, the standard universal quasi-chemical functional group activity coefficients (UNIFAC) within E-AIM can be used to predict a_w, σ_{sol}, and ρ_{sol} of organic aqueous solution (Fredenslund et al., 1975; Hansen et al., 1991). Note that the E-AIM calculations based on the standard UNIFAC group contribution method predict hygroscopic growth factors of organic aerosol particles. (i.e.., E-AIM model (standard UNIFAC)) growth curve as a function of RH is based on Eq. (1) and Eq. (6).).

$$G_f = \left(\frac{\rho_s}{x_s \rho_{sol}}\right)^{\frac{1}{3}} \quad (6)$$

ρ_s and ρ_{sol} are the density of solute and solution, respectively, and x_s is the solute mass fraction.

3 Results and discussion

3.1 Levoglucosan

3.1.1 Concentration-dependent water activity of levoglucosan solution

By applying a water activity parameterization model (KD, Eq. 3) to measured growth factors of levoglucosan aerosol nanoparticles with diameters from 20 to 100 nm using a nano-HTDMA, as shown in Fig. 2, we obtain water activity of aqueous levoglucosan nanoparticles with molality up to 140 mol kg^{-1}. Chan et al. (2005) levitated single particles of ~10 μm levoglucosan at the different RHs in an electrodynamic balance for mass measurements, and reported water activity data for aqueous droplets with molality up to 14 mol kg^{-1}. These water activity data are compared with predictions from the Köhler (Kreidenweis et al., 2005, Eq. 2) and the E-AIM model, respectively. A good agreement between KD-derived water activity and Köhler indicates these aerosol particles are aqueous droplets with molality less than 20 mol kg^{-1}. However, a derivation of SKT from the KD-derived water activity is observed as the molality increases from 20 to 120 mol kg^{-1}, indicating levoglucosan nanoparticles become highly supersaturated. Also, a discrepancy exists between KD-derived data and E-AIM model prediction. For DKA-derived water activity calculations, a strong size dependence of the hygroscopic growth factors is needed for aerosol nanoparticles in the different sizes, which is not the case for the hygroscopic measurements of levoglucosan nanoparticles.

3.1.2 Size dependent hygroscopicity of levoglucosan nanoparticles

Black solid squares in Fig. 3 shows the measured humidogram of 100-nm levoglucosan nanoparticles in both deliquescence and efflorescence modes. Levoglucosan nanoparticles uptake water continuously from 5 % to 90 % RH. Also, they gradually release water as RH decreases down to 5 %. The hygroscopic growth factors of levoglucosan nanoparticles in deliquescence and efflorescence modes overlap. For example, the hygroscopic growth factors of levoglucosan nanoparticles at 80 % RH, 87 % RH are 1.16, 1.23, respectively, in the deliquescence mode, very close to the corresponding values in the efflorescence mode at the same RH (shown in Fig. S1),

suggesting that growing and shrinking of particles are in equilibrium. No prompt phase transitions of levoglucosan nanoparticles are observed in both deliquescence and efflorescence modes. A similar non-prompt phase transition of levoglucosan nanoparticles was observed in the previous studies (Mochida and Kawamura, 2004; Chan et al., 2005; Svenningsson et al., 2006; Mikhailov et al., 2008; Lei et al., 2014, 2018). This study is in good agreement with most of reference results, but there is a difference in the hygroscopic growth factor of levoglucosan nanoparticles between Mikhailov et al. (2008) and this study. The reason is that Mikhailov et al. (2008) used minimum mobility diameter measured in the deliquescence and efflorescence modes instead of the initial dry mobility diameter measured in the deliquescence or efflorescence modes to calculate the hygroscopic growth factor of levoglucosan nanoparticles, which could lead to the higher hygroscopic growth factors of levoglucosan nanoparticles than those of this study.

Figure 4 shows measured size-resolved hygroscopic growth factors of levoglucosan nanoparticles against RH up to 90 %. There is a weak size dependence of hygroscopic growth factors of levoglucosan nanoparticles with diameters down to 20 nm in both deliquescence and efflorescence modes. E.g., a slight difference in hygroscopic growth factor between 100 and 20 nm levoglucosan nanoparticles is ~0.02 at 88 % RH. In addition, E-AIM (standard UNIFAC) model and ideal solution theory are used to predict our measurement results as shown in Fig. 4a and 4b, respectively. E-AIM (standard UNIFAC) model is applied to estimate the hygroscopic growth of organic aerosol nanoparticles according to UNIFAC group contribution method. Ideal solution theory is used to describe water absorption of the ideal/diluted aqueous solution nanodroplets. Due to consideration of Kelvin effect in model and theory, these model predictions are expected to present a size dependence of growth factors of nanoparticles in size from 100 down to 20 nm. For example, as shown in Fig. 4a, for levoglucosan nanoparticles with diameters of 100, 60, and 20 nm, the

thermodynamic equilibrium model (E-AIM (standard UNIFAC)) shows a weak size dependence of the growth factors at low RH but a strong size dependence of growth factors at RH above 70 %. However, the calculated growth factors of nanoparticles down to 20 nm in size are deviated from the measured growth factors of levoglucosan nanoparticles at RH below 80 %, which is similar to the observation of 100-nm levoglucosan hygroscopicity prediction from previous studies (Lei et al., 2014, 2018). Lei et al. (2014, 2018) explained that the possible reason for this discrepancy is that the E-AIM (standard UNIFAC) predictions are not suitable for organic compounds with the strongly polar functional groups in series (Fredenslund et al., 1975; Hansen et al., 1991). Since levoglucosan contains three OH groups in series, thus, thermodynamic properties (e.g., water activity, surface tension) in E-AIM (standard UNIFAC) are more likely to be invalid for levoglucosan system. However, a good agreement of growth factors of levoglucosan with diameters 100, 60, and 20 nm is observed between measurements and predictions by ideal solution theory as shown in Fig. 4b.

The hygroscopic growth for sub-20 nm levoglucosan nanoparticles cannot be determined with the nano-HTDMA system because we observed significant evaporation of the dry particles in the measurement system. Figure 5a-b shows the measured peak diameter of normalized size distribution scanned by the nano-DMA2 and nano-DMA1 for sub-20 nm levoglucosan nanoparticles. It is obvious that the size of nanoparticles in DMA2 is smaller than that in DMA1, corresponding to a decrease of 22 % to 50 % of 15 and 10 nm levoglucosan nanoparticles, respectively, indicating significant evaporation of these small levoglucosan nanoparticles in the system. To test this hypothesis, we estimate the ratio of gas-phase concentration to the total concentration of the generated levoglucosan nanoparticles in the different sizes. Firstly, the calculated gas-phase concentration of levoglucosan is based on the Kelvin equation and ideal gas

equation (Eq. S1&2, SI. S1). Figure 5c shows the vapor saturation ratio of levoglucosan as nanodroplet diameter increases from1 to 100 nm. The inset in Fig. 5c is an enlarged view (black open square) of vapor saturation ratio of levoglucosan as a function of nanodroplet diameters below 20 nm. Levoglucosan is semi-volatile at ambient condition (Hennigan et al., 2010). Due to Kelvin effect, sub-20 nm levoglucosan aerosol particles become more volatile. Secondly, the total concentration of levoglucosan particles is estimated by Eq. (S3). The results of the ratio of gas-phase concentration (m_g) to the total concentration (m_t) have been shown in Fig. 5d and Table S3 for levoglucosan nanoparticles in the diameter range from 10 to 100 nm. It shows a slight increase in the calculated ratio (m_g/m_t) for levoglucosan aerosol nanoparticles with dimeters from 100 down to 20 nm. However, the ratio of gas-phase concentration to the total concentration is dramatically enhanced for sub-20 nm levoglucosan aerosol nanoparticles, which is consistent with measurement observations, indicating the larger impact of evaporation of sub-20 nm levoglucosan nanoparticles on the measurement results. Therefore, there is the obvious partial levoglucosan evaporation from DMA1 to DMA2 within several seconds.

3.2 D-glucose

3.2.1 Concentration-dependent water activity of D-glucose solution

Figure 6 shows the DKA-derived water activity of aqueous D-glucose nanodroplets with diameters from 6 nm to 100 nm with molality up to 1000 mol kg^{-1} (Cheng et al., 2015, Eq. 4). Here, by comparing with KD-derived water activity, Köhler, E-AIM model, and observation from literatures (Comesaña et al., 2001; Peng et al., 2001; Bhandari and Bareyre, 2003; Ferreira et al., 2003), a good agreement among them is observed in the solute concentration below 20 mol kg^{-1}. However,

there is a disagreement between water activity results in the highly supersaturated concentration range (> 20 mol kg^{-1}).

3.2.2 Size dependent hygroscopicity of D-glucose nanoparticles

Figure 7 shows the measured hygroscopic growth factors of 100-nm D-glucose nanoparticles as a function of RH. No significant difference in the hygroscopic growth factor of 100-nm D-glucose nanoparticles is found between deliquescence and efflorescence measurement modes (Fig. S2). For example, the measured growth factors of D-glucose nanoparticles at 81 % RH, 88 % RH are 1.16, 1.25 in the deliquescence mode, respectively, in good agreement with results in the efflorescence mode (g_f =1.17 at 81 % RH, g_f =1.26 at 88 % RH shown in Fig. S2). Also, measured hygroscopic growth factors of 100-nm D-glucose are consistent with results from previous studies (Mochida and Kawamura. 2004; Chan and Chan, 2005; Suda and Petters, 2013; Estillore et al., 2017; Mikhailov and Vlasenko, 2020). For example, Mikhailov and Vlasenko, (2020) investigated the hygroscopic behavior of 100-nm D-glucose aerosol particles using a HHTDMA in deliquescence, efflorescence, and restructuring modes of operation, respectively. A clear morphology effect on the hygroscopicity of D-glucose aerosol particles is observed in the RH range from 2 % to 96 % RH. No prompt phase transitions are observed in both deliquescence and efflorescence measurement modes. Estillore et al. (2017) observed a slightly amorphous structure of D-glucose particles under ambient conditions using an atomic force microscopy and D-glucose particles grow through gradual water uptake. Thus, a continuous growth/shrink of diameter in both deliquescence and efflorescence modes is explained by the lack of crystallization of D-glucose nanoparticles upon drying to low RH below 10 %.

Figure 8a shows the size dependence of measured hygroscopic growth factors of D-glucose nanoparticles in the size range from 6 to 100 nm, with differences in growth factor up to 0.14

between 100-nm and 6-nm nanoparticles at 90 % RH (Fig. S2). A weak size dependence on the hygroscopic growth factors of D-glucose nanoparticles is observed in the size range from 20 to 100 nm, which is similar to observation for levoglucosan nanoparticles with diameters down to 20 nm. However, there is a strong size-dependent growth factor of D-glucose nanoparticles with diameters from 6 to 20 nm, especially at high RH, i.e., RH > ~80%. There is no evident difference in hygroscopic growth factors of D-glucose nanoparticles at RH below 80 % in size range from 6 to 100 nm. The reason that the growth factor shows size dependence only in the regime of hygroscopic growth (RH > ～80%), and not in the regime of water adsorption (RH < ～80%) has not been explained before. Our hypothesis is that the distinct behaviors between high RH and low RH region can be attributed to the distinct size effect on the hygroscopic growth and adsorption, i.e., the growth factor shows size dependence only in the regime of hygroscopic growth (RH > ～80 %), and not in the regime of water adsorption (RH < ～80 %). Figure 8b further shows the clear change in the hygroscopic growth factor of D-glucose aerosol nanoparticles with diameters from 100 down to 6 nm at 87 % RH. The hygroscopic growth factor of D-glucose nanoparticles is almost unchanged with diameters from 20 to 100 nm. However, a markedly increase in the hygroscopic growth factor of D-glucose aerosol nanoparticles is observed as size increases from 6 to 20 nm. E-AIM model predict well the measured hygroscopic growth factors of D-glucose with diameters smaller than 15 nm at 87 % RH, while ideal solution theory agrees with hygroscopic measurement results of D-glucose with diameters higher than 60 nm at the same RH. The use of DKA methods leads to a good agreement between measurements and model predictions.

The measured hygroscopic growth factors of D-glucose nanoparticles with diameters of 6 and 100 nm are compared with the model and theory shown in Fig. 9, Fig. S3, and Fig. S4, respectively. Ideal solution theory is applied to predict the hygroscopic growth factor of organics in the ideal

solution. Figure 9a and Fig. S3 show that the measured growth factors of 100-nm D-glucose nanoparticles are lower than predicted growth factors from E-AIM (standard UNIFAC) model, especially at RH below 85 %. Also, E-AIM (standard UNIFAC) model could predict well the measured hygroscopic growth factor of 6-nm D-glucose aerosol nanoparticles at RH above 40 % shown in Fig. 9a and Fig. S3. The possible reason for discrepancies between E-AIM (standard UNIFAC) model and measurements is inaccurate thermodynamic parameters (e.g., water activity, surface tension) estimated by the E-AIM (standard UNIFAC) model without consideration intramolecular interaction (Fredenslund et al., 1975; Hansen et al., 1991; Fredenslund and Sørensen, 1994; Mochida and Kawamura, 2004). D-glucose contains five OH groups in series, hydrogen bond could potentially exist and affects the E-AIM (standard UNIFAC) model-measurement agreement for D-glucose aerosol nanoparticles system (Mochida and Kawamura, 2004; Lei et al., 2014, 2018). The ideal solution theory is used to predict the hygroscopic curve of D-glucose nanoparticles with diameters of 6-100 nm, shown in Fig. 9b and Fig. S3. There is a good agreement between measured growth factors of 100-nm D-glucose and ideal theory predictions. This suggests that thermodynamic parameters (e.g., water activity, surface tension, and solution density) assumed by the ideal solution theory are accurate to use in Eq. (1) and (2) for predicting the hygroscopic curve of D-glucose nanoparticles with large sizes (e.g., 60, 100 nm). However, an underestimation of growth factors of 6-nm D-glucose nanoparticles has been shown in Fig. 9b and Fig. S3 by ideal solution theory prediction at RH above 30 %. For ideal solution, water activity of liquid droplets can be simply estimated from the mole fraction of water. With from 20 down to 6 nm, D-glucose nanodroplets can be highly supersaturated, and the water activity is not equal to mole fraction of water. Thus, with the assumption of idea solution, the model failed to predict the observed growth factors of 6-nm D-glucose nanoparticles at RH above 30 %. However, the current thermodynamic

models (e.g., E-AIM) mostly rely on the concentration-dependent thermodynamic properties (such as water activity) derived from the measurements of large aerosol particles or even bulk samples (Tang and Munkelwitz, 1994; Tang, 1996; Pruppacher and Klett, 1997; Clegg et al., 1998). They are thus difficult or impossible to apply to describe the hygroscopic behavior of sub-10 nm nanoparticles, which can often be supersaturated in concentration compared to bulk solutions (Cheng et al., 2015; Wang et al., 2018). Thus, nanosize effect on these thermodynamic properties has been taken into account the models and theories (Cheng et al., 2015). Combination of DKA methods and hygroscopic measurements of aerosol nanoparticles in the different sizes can use to determine the thermodynamic properties (e.g., water activity) in the highly supersaturated concentration range (Cheng et al., 2015). Therefore, as shown in Fig. 9c and Fig. S4, the use of the DKA method leads a good agreement with the measured hygroscopic growth factors of Glucose nanoparticles with diameters from 100 down to 6 nm.

4 Conclusions

In this study, we investigate the hygroscopic behavior of levoglucosan and D-glucose nanoparticles with diameters down to 6 nm using a nano-HTDMA. Due to the larger impact of evaporation of sub-20 nm levoglucosan nanoparticles in the nano-HTDMA system, we measure hygroscopic growth factor of levoglucosan with diameters down to 20 nm. There is a weak size dependence of hygroscopic growth factor of levoglucosan and D-glucose with diameters down to 20 nm, while a strong size dependence of the hygroscopic growth factor of D-glucose has been clearly observed in the size range from 6 to 20 nm. No prompt phase transitions occur in both deliquescence and efflorescence modes for both levoglucosan and D-glucose nanoparticles. By comparing with the KD-derived water activity, Köhler, E-AIM model, and DKA-derived data, the predicted water

activity of aqueous organic solution (levoglucosan and D-glucose) is consistent with observation data from references in the low solute concentration (< 20 mol kg^{-1}) but failed in the solute concentration (> 20 mol kg^{-1}). In addition, ideal solution theory predicts well the hygroscopic behavior of two specific organics with diameters higher than 60 nm (levoglucosan and D-glucose), while hygroscopic growth factor of D-glucose down to 6 nm in size is in good agreement with E-AIM (standard UNIFAC) model prediction at high RH. The use of the DKA method leads to a good agreement with measured hygroscopic growth factor of glucose nanoparticles with diameters from 100 down to 6 nm.

Data availability

Reader who are interested in the data should contact Yafang Cheng (Yafang.cheng@mpic.de).

Competing interests

Some authors are members of the editorial board of journal Atmospheric Chemistry Physics. The peer-review process was guided by an independent editor, and the authors have also no other competing interests to declare

Acknowledgement

This study was supported by the Max Planck Society (MPG) and Leibniz Society. T.L acknowledges the support from China Scholarship Council (CSC). Y. C. would like to acknowledge the Minerva Program of MPG.

Author contributions: Y.C. and H.S. designed and led the study. T.L. performed the experiments. All co-authors discussed the results and commented on the manuscript. T.L. wrote the manuscript with input from all co-authors.

4 References

Andreae, M. O. and Gelencsér, A.: Black carbon or brown carbon? The nature of light-absorbing carbonaceous aerosols, Atmos. Chem. Phys., 6, 3131–3148, https://doi.org/10.5194/acp-6-3131-2006, 2006.

Bhandari, B. and Bareyre, I.: Estimation of crystalline phase present in the glucose crystal–solution mixture by water activity measurement, LWT - Food Science and Technology, 36, 729-733, 2003.

Bhattarai, H., Saikawa, E., Wan, X., Zhu, H., Ram, K., Gao, S., Kang, S., Zhang, Q., Zhang, Y., Wu, G., Wang, X., Kawamura, K., Fu, P., and Cong, Z.: Levoglucosan as a tracer of biomass burning: Recent progress and perspectives, Atmos. Res., 220, 20–33, 2019.

Biskos, G., Malinowski, A., Russell, L. M., Buseck, P. R., and Martin, S. T.: Nanosize effect on the deliquescence and the efflorescence of sodium chloride particles, Aerosol Sci. Technol., 40, 97-106, 2006a.

Biskos, G., Paulsen, D., Russell, L. M., Buseck, P. R., and Martin, S. T.: Prompt deliquescence and efflorescence of aerosol nanoparticles, Atmos. Chem. Phys., 6, 4633–4642, https://doi.org/10.5194/acp-6-4633-2006, 2006b.

Biskos, G., Russell, L. M., Buseck, P. R., and Martin, S. T.: Nanosize effect on the hygroscopic growth factor of aerosol particles, Geophys. Res. Lett., 33, L07801, doi:10.1029/2005GL025199, 2007.

Bohren, C. and Huffmann, D.: Absorption and scattering of light by small particles, Wiley-VCH, New York, USA, 2004.

Bzdek, B. R., Zordan, C. A., Luther, G. W., and Johnston, M. V.: Nanoparticle Chemical Composition During New Particle Formation, Aerosol Science and Technology, 45, 1041-1048, 2011.

Chan, M. N., Choi, M. Y., Ng, N. L., and Chan, C. K.: Hygroscopicity of water-soluble organic compounds in atmospheric aerosols: Amino acids and biomass burning derived organic species, Environ. Sci. Technol., 39, 1555-1562, 2005.

Chan, M. N. and Chan, C. K.: Mass transfer effects in hygroscopic measurements of aerosol particles, Atmos. Chem. Phys., 5, 2703–2712, https://doi.org/10.5194/acp-5-2703-2005, 2005.

Charlson, R. J., Schwartz, S. E., Hales, J. M., Cess, R. D., Coakley, J. A., Hansen, J. E., and Hoffmann, D. J.: Climate forcing by anthropogenic aerosols, Science, 255, 423-430, 1992.

Chen, Da-Ren, David Y.H. Pui, and Stanley L. Kaufman.: Electrospraying of conducting liquids for monodisperse aerosol generation in the 4 nm to 1.8 nm diameter range, J. Aerosol Sci., 26:963-977.

Cheng, Y. F., Su, H., Koop, T., Mikhailov, E., and Pöschl, U.: Size dependence of phase transitions in aerosol nanoparticles, Nat. Commun., 6, 5923, doi:10.1038/ncomms6923, 2015.

Cheng, Y. F., Su, H., Rose, D., Gunthe, S. S., Berghof, M., Wehner, B., Achtert, P., Nowak, A., Takegawa, N., Kondo, Y., Shiraiwa, M., Gong, Y. G., Shao, M., Hu, M., Zhu, T., Zhang, Y. H., Carmichael, G. R., Wiedensohler, A., Andreae, M. O., and Pöschl, U.: Size-resolved measurement of the mixing state of soot in the megacity Beijing, China: diurnal cycle, aging and parameterization, Atmos. Chem. Phys., 12, 4477–4491, https://doi.org/10.5194/acp-12-4477-2012, 2012.

462 Chýlek, P. and Coakley, J. A.: Aerosols and climate, Science, 183, 75-77, 1974.
463 Clegg, S. L., Brimblecombe, P., and Wexler, A. S.: Thermodynamic model of the system
464 H+−NH4+−SO42-−NO3-−H2O at tropospheric temperatures, J. Phys. Chem. A, 102, 2137–
465 2154, doi:10.1021/Jp973042r, 1998.
466 Clegg, S. L., Seinfeld, J. H., and Brimblecombe, P.: Thermody-namic modelling of aqueous
467 aerosols containing electrolytes and dissolved organic compounds, J. Aerosol Sci., 32, 713–
468 738, doi:10.1016/s0021-8502(00)00105-1, 2001.
469 Clegg, S. L. and Seinfeld, J. H.: Thermodynamic models of aqueous solutions containing in-
470 organic electrolytes and dicarboxylic acids at 298.15 K. 2. Systems including dissociation
471 equilibria, J. Phys. Chem. A, 110, 5718–5734, doi:10.1021/jp056150j, 2006.
472 Comesaña, J. F., Correa, A., and Sereno, A. M.: Water activity at 35 °C in 'sugar' + water and
473 'sugar' + sodium chloride + water systems, Int. J. Food Sci. Tech., 36, 655-661, 2001.
474 Dick, W. D., Saxena, P., and McMurry, P. H.: Estimation of water uptake by organic compounds
475 in submicron aerosols measured during the Southeastern Aerosol and Visibility Study, J. Geo-
476 phys. Res.-Atmos., 105, 1471–1479, doi:10.1029/1999jd901001, 2000.
477 Dunne, E. M., Gordon, H., Kürten, A., Almeida, J., Duplissy, J., Williamson, C., Ortega, I. K.,
478 Pringle, K. J., Adamov, A., Baltensperger, U., Barmet, P., Benduhn, F., Bianchi, F.,
479 Breitenlechner, M., Clarke, A., Curtius, J., Dommen, J., Donahue, N. M., Ehrhart, S., Flagan,
480 R. C., Franchin, A., Guida, R., Hakala, J., Hansel, A., Heinritzi, M., Jokinen, T., Kangasluoma,
481 J., Kirkby, J., Kulmala, M., Kupc, A., Lawler, M. J., Lehtipalo, K., Makhmutov, V., Mann,
482 G., Mathot, S., Merikanto, J., Miettinen, P., Nenes, A., Onnela, A., Rap, A., Reddington, C.
483 L. S., Riccobono, F., Richards, N. A. D., Rissanen, M. P., Rondo, L., Sarnela, N.,
484 Schobesberger, S., Sengupta, K., Simon, M., Sipilä, M., Smith, J. N., Stozkhov, Y., Tomé, A.,

Tröstl, J., Wagner, P. E., Wimmer, D., Winkler, P. M., Worsnop, D. R., and Carslaw, K. S.: Global atmospheric particle formation from CERN CLOUD measurements, Science., 354, 1119-1124, 2016.

Duplissy, J., Gysel, M., Sjogren, S., Meyer, N., Good, N., Kammermann, L., Michaud, V., Weigel, R., Martins dos Santos, S., Gruening, C., Villani, P., Laj, P., Sellegri, K., Metzger, A., McFiggans, G. B., Wehrle, G., Richter, R., Dommen, J., Ristovski, Z., Baltensperger, U., and Weingartner, E.: Intercomparison study of six HTDMAs: results and recommendations, Atmos. Meas. Tech., 2, 363–378, https://doi.org/10.5194/amt-2-363-2009, 2009.

Dusek, U., Frank, G. P., Curtius, J., Drewnick, F., Schneider, J., Kürten, A., Rose, D., Andreae, M. O., Borrmann, S., and Pöschl, U.: Enhanced organic mass fraction and decreased hygroscopicity of cloud condensation nuclei (CCN) during new particle formation events, Geophys. Res. Lett., 37, 2010.

Dutcher, C. S., Ge, X., Wexler, A. S. & Clegg, S. L. An Isotherm-Based Thermodynamic Model of Multicomponent Aqueous Solutions, Applicable Over the Entire Concentration Range. J. Phys. Chem. A 117, 3198-3213 (2013).

Elias, V. O., Simoneit, B. R. T., Cordeiro, R. C., and Turcq, B.: Evaluating levoglucosan as an indicator of biomass burning in Carajás, amazônia: a comparison to the charcoal record22Associate editor: R. Summons, Geochim. Cosmochim. Acta., 65, 267-272, 2001.

Estillore, A. D., Morris, H. S., Or, V. W., Lee, H. D., Alves, M. R., Marciano, M. A., Laskina, O., Qin, Z., Tivanski, A. V., and Grassian, V. H.: Linking hygroscopicity and the surface microstructure of model inorganic salts, simple and complex carbohydrates, and authentic sea spray aerosol particles, Phys. Chem. Chem. Phys., 19, 21101-21111, 2017.

Ferreira, O., Brignole, E. A., and Macedo, E. A.: Phase equilibria in sugar solutions using the A-UNIFAC model, Ind. Eng. Chem. Res., 42 (24), 6212–6222, 2003.

Fraser, M. P. and Lakshmanan, K.: Using Levoglucosan as a Molecular Marker for the Long-Range Transport of Biomass Combustion Aerosols, Environ. Sci. Technol., 34, 4560-4564, 2000.

Fredenslund, A., Jones, R. L., and Prausnitz, J. M.: Group-contribution estimation of activity-coefficients in nonideal liquid-mixtures, Aiche J., 21, 1086–1099, doi:10.1002/aic.690210607, 1975.

Hämeri, K., Laaksonen, A., Väkevä, M., and Suni, T.: Hygroscopic growth of ultrafine sodium chloride particles, J. Geophys. Res., 106, 20 749–20 757, 2001.

Hämeri, K., Väkevä, M., Hansson, H.-C., and Laaksonen, A.: Hygroscopic growth of ultrafine ammonium sulfate aerosol measured using an ultrafine tandem differential mobility analyzer, J. Geophys. Res., 105, 22 231–22 242, 2000.

Hansen, H. K., Rasmussen, P., Fredenslund, A., Schiller, M., and Gmehling, J.: Vapor–liquid equilibria by UNIFAC group contribution. 5. Revision and extension, Ind. Eng. Chem. Res., 30, 2352–2355, doi:10.1021/ie00058a017, 1991.

Hennigan, Christopher J.; Sullivan, Amy P.; Collett, Jeffrey L.; Robinson, Allen L., Levoglucosan stability in biomass burning particles exposed to hydroxyl radicals. Geophysical Research Letters, 37(9), doi:10.1029/2010gl043088, 2010.

Kerminen, V.-M.: The effects of particle chemical character and atmospheric processes on particle hygroscopic properties, J. Aerosol Sci., 28, 121–132, 1997.

Keskinen, H., Virtanen, A., Joutsensaari, J., Tsagkogeorgas, G., Duplissy, J., Schobesberger, S., Gysel, M., Riccobono, F., Slowik, J. G., Bianchi, F., Yli-Juuti, T., Lehtipalo, K., Rondo, L., Breitenlechner, M., Kupc, A., Almeida, J., Amorim, A., Dunne, E. M., Downard, A. J.,

Ehrhart, S., Franchin, A., Kajos, M. K., Kirkby, J., Kürten, A., Nieminen, T., Makhmutov, V., Mathot, S., Miettinen, P., Onnela, A., Petäjä, T., Praplan, A., Santos, F. D., Schallhart, S., Sipilä, M., Stozhkov, Y., Tomé, A., Vaattovaara, P., Wimmer, D., Prevot, A., Dommen, J., Donahue, N. M., Flagan, R. C., Weingartner, E., Viisanen, Y., Riipinen, I., Hansel, A., Curtius, J., Kulmala, M., Worsnop, D. R., Baltensperger, U., Wex, H., Stratmann, F., and Laaksonen, A.: Evolution of particle composition in CLOUD nucleation experiments, Atmos. Chem. Phys., 13, 5587–5600, https://doi.org/10.5194/acp-13-5587-2013, 2013.

Kim, J., Ahlm, L., Yli-Juuti, T., Lawler, M., Keskinen, H., Tröstl, J., Schobesberger, S., Duplissy, J., Amorim, A., Bianchi, F., Donahue, N. M., Flagan, R. C., Hakala, J., Heinritzi, M., Jokinen, T., Kürten, A., Laaksonen, A., Lehtipalo, K., Miettinen, P., Petäjä, T., Rissanen, M. P., Rondo, L., Sengupta, K., Simon, M., Tomé, A., Williamson, C., Wimmer, D., Winkler, P. M., Ehrhart, S., Ye, P., Kirkby, J., Curtius, J., Baltensperger, U., Kulmala, M., Lehtinen, K. E. J., Smith, J. N., Riipinen, I., and Virtanen, A.: Hygroscopicity of nanoparticles produced from homogeneous nucleation in the CLOUD experiments, Atmos. Chem. Phys., 16, 293–304, https://doi.org/10.5194/acp-16-293-2016, 2016.

Koehler, K. A., Kreidenweis, S. M., DeMott, P. J., Prenni, A. J., Carrico, C. M., Ervens, B., and Feingold, G.: Water activity and activation diameters from hygroscopicity data - Part II: Application to organic species, Atmos. Chem. Phys., 6, 795-809, 2006.

Köhler, H.: The nucleus in and the growth of hygroscopic droplets, Trans. Faraday Soc., 32, 1152–1161, 1936.

Kreidenweis, S. M., Koehler, K., DeMott, P. J., Prenni, A. J., Carrico, C., and Ervens, B.: Water activity and activation diameters from hygroscopicity data - Part I: Theory and application to

552 inorganic salts, Atmos. Chem. Phys., 5, 1357–1370, https://doi.org/10.5194/acp-5-1357-2005,
553 2005.
554 Kulmala, M., Kontkanen, J., Junninen, H., Lehtipalo, K., Manninen, H. E., Nieminen, T., Petäjä,
555 T., Sipilä, M., Schobesberger, S., Rantala, P., Franchin, A., Jokinen, T., Järvinen, E., Äijälä,
556 M., Kangasluoma, J., Hakala, J., Aalto, P. P., Paasonen, P., Mikkilä, J., Vanhanen, J., Aalto,
557 J., Hakola, H., Makkonen, U., Ruuskanen, T., Mauldin, R. L., Duplissy, J., Vehkamäki, H.,
558 Bäck, J., Kortelainen, A., Riipinen, I., Kurtén, T., Johnston, M. V., Smith, J. N., Ehn, M.,
559 Mentel, T. F., Lehtinen, K. E. J., Laaksonen, A., Kerminen, V.-M., and Worsnop, D. R.: Direct
560 Observations of Atmospheric Aerosol Nucleation, Science, 339, 943-946, 2013.
561 Lei, T., Ma, N., Hong, J., Tuch, T., Wang, X., Wang, Z., Pöhlker, M., Ge, M., Wang, W., Mikhailov,
562 E., Hoffmann, T., Pöschl, U., Su, H., Wiedensohler, A., and Cheng, Y.: Nano-hygroscopicity
563 tandem differential mobility analyzer (nano-HTDMA) for investigating hygroscopic
564 properties of sub-10 nm aerosol nanoparticles, Atmos. Meas. Tech., 13, 5551–5567,
565 https://doi.org/10.5194/amt-13-5551-2020, 2020
566 Lei, T., Zuend, A., Cheng, Y., Su, H., Wang, W., and Ge, M.: Hygroscopicity of organic surrogate
567 compounds from biomass burning and their effect on the efflorescence of ammonium
568 sulfate in mixed aerosol particles, Atmos. Chem. Phys., 18, 1045-1064, 2018.
569 Lei, T., Zuend, A., Wang, W. G., Zhang, Y. H., and Ge, M. F.: Hygroscopicity of organic
570 compounds from biomass burning and their influence on the water uptake of mixed organic
571 ammonium sulfate aerosols, Atmos. Chem. Phys., 14, 11165-11183, 2014.
572 Lihavainen, H., Kerminen, V.-M., Komppula, M., Hatakka, J., Aaltonen, V., Kulmala, M., and
573 Viisanen, Y.: Production of “potential” cloud condensation nuclei associated with

574 atmospheric new-particle formation in northern Finland, J. Geophys. Res., 108, 4782,
575 doi:10.1029/2003JD003887, 2003.
576 Mikhailov, E., Vlasenko, S., Martin, S. T., Koop, T., and Pöschl, U.: Amorphous and crystalline
577 aerosol particles interacting with water vapor: conceptual framework and experimental
578 evidence for restructuring, phase transitions and kinetic limitations, Atmos. Chem. Phys., 9,
579 9491–9522, https://doi.org/10.5194/acp-9-9491-2009, 2009.
580 Mikhailov, E. F. and Vlasenko, S. S.: High humidity tandem differential mobility analyzer for
581 accurate determination of aerosol hygroscopic growth, microstructure and activity
582 coefficients over a wide range of relative humidity, Atmos. Meas. Tech., 13, 2035–2056,
583 https://doi.org/10.5194/amt-13-2035-2020, 2020.
584 Mikhailov, E. F., Vlasenko, S. S., and Ryshkevich, T. I.: Influence of chemical composition and
585 microstructure on the hygroscopic growth of pyrogenic aerosol, Izv. Atmos. Ocean. Phy., 44,
586 416–431, 2008.
587 Mochida, M. and Kawamura, K.: Hygroscopic properties of levoglucosan and related organic
588 compounds characteristic to biomass burning aerosol particles, J. Geophys. Res.-Atmos., 109,
589 D21202, doi:10.1029/2004jd004962, 2004.
590 Peng, C., Chow, A. H. L., and Chan, C. K.: Hygroscopic study of glucose, citric acid, and sorbitol
591 using an electrodynamic balance: comparison with UNIFAC Predictions, Aerosol Sci.
592 Technol., 35 (3), 753–758, 2001.
593 Pruppacher, H. R. and Klett, J. D: Microphysics of clouds and precipitation, Kluwer Academic
594 Publishers, 1997.
595 Pöhlker, M. L., Pöhlker, C., Ditas, F., Klimach, T., Hrabe de Angelis, I., Araújo, A., Brito, J.,
596 Carbone, S., Cheng, Y., Chi, X., Ditz, 105 R., Gunthe, S. S., Kesselmeier, J., Könemann, T.,

Lavriˇc, J. V., Martin, S. T., Mikhailov, E., Moran-Zuloaga, D., Rose, D., Saturno, J., Su, H., Thalman, R., Walter, D., Wang, J., Wolff, S., Barbosa, H. M. J., Artaxo, P., Andreae, M. O., and Pöschl, U.: Longterm observations of cloud condensation nuclei in the Amazon 110 rain forest – Part 1: Aerosol size distribution, hygroscopicity, and new model parametrizations for CCN prediction, Atmos. Chem. Phys., 16, 15709–15740, https://doi.org/10.5194/acp-16-157092016, 2016

Raoux, S., Rettner, C. T., Jordan-Sweet, J. L., Kellock, A. J., Topuria, T., Rice, P. M., and Miller, D. C.: Direct observation of amorphous to crystalline phase transitions in nanoparticle arrays of phase change materials, J. Appl. Phys., 102, 094305 (2007).

Randles, C. A., Russell, L. M., and Ramaswamy, V.: Hygroscopic and optical properties of organic sea salt aerosol and consequences for climate forcing, Geophys. Res. Lett., 31, L16 108, doi:10.1029/2004GL020628, 2004.

Seinfeld, J. H., and Pandis, S. N.: Atmospheric Chemistry and Physics: From Air Pollution to Climate Change (Second edition), Wiley Interscience, New York, 2006.

Sihto, S. L., Mikkilä, J., Vanhanen, J., Ehn, M., Liao, L., Lehtipalo, K., Aalto, P. P., Duplissy, J., Petäjä, T., Kerminen, V. M., Boy, M., and Kulmala, M.: Seasonal variation of CCN concentrations and aerosol activation properties in boreal forest, Atmos. Chem. Phys., 11, 13269-13285, https://doi.org/10.5194/acp-11-13269-2011, 2011.

Simoneit, B. R. T., Schauer, J. J., Nolte, C. G., Oros, D. R., Elias, V. O., Fraser, M. P., Rogge, W. F., and Cass, G. R.: Levoglucosan, a tracer for cellulose in biomass burning and atmospheric particles, Atmos. Environ, 33, 173-182, 1999.

Suda, S. R. and Petters, M. D.: Accurate determination of aerosol activity coefficients at relative humidities up to 99 % using the hygroscopicity tandem differential mobility analyzer

technique, Aerosol Sci. Technol., 47, 991–1000, https://doi.org/10.1080/02786826.2013.807906, 2013.

Su, H., Rose, D., Cheng, Y. F., Gunthe, S. S., Massling, A., Stock, M., Wiedensohler, A., Andreae, M. O., and Pöschl, U.: Hygroscopicity distribution concept for measurement data analysis and modeling of aerosol particle mixing state with regard to hygroscopic growth and CCN activation, Atmos. Chem. Phys., 10, 7489–7503, https://doi.org/10.5194/acp-10-7489-2010, 2010.

Svenningsson, B., Rissler, J., Swietlicki, E., Mircea, M., Bilde, M., Facchini, M. C., Decesari, S., Fuzzi, S., Zhou, J., Mønster, J., and Rosenørn, T.: Hygroscopic growth and critical supersaturations for mixed aerosol particles of inorganic and organic compounds of atmospheric relevance, Atmos. Chem. Phys., 6, 1937-1952, 2006.

Tang, I. N.: Chemical and size effects of hygroscopic aerosols on light scattering coefficients, J. Geophys. Res., 101, 19 245– 19 250, 1996.

Tang, I. N., Fung, K. H., Imre, D. G., and Munkelwitz, H. R.: Phase Transformation and Metastability of Hygroscopic Microparticles, J. Geophys. Res.-Atmos, 99, 18801– 18808, 1994.

Wang, J., Shilling, J. E., Liu, J., Zelenyuk, A., Bell, D. M., Petters, M. D., Thalman, R., Mei, F., Zaveri, R. A., and Zheng, G.: Cloud droplet activation of secondary organic aerosol is mainly controlled by molecular weight, not water solubility, Atmos. Chem. Phys., 19, 941-954, 2019.

Wang, Z., Cheng, Y., Ma, N., Mikhailov, E., Pöschl, U., and Su, H.: Dependence of the hygroscopicity parameter κ on particle size, humidity and solute concentration: implications for laboratory experiments, field measurements and model studies, Atmos. Chem. Phys. Discuss., 2017, 1-33, 2017.

643 Wang, Z., Su, H., Wang, X., Ma, N., Wiedensohler, A., Pöschl, U., and Cheng, Y.: Scanning
644 supersaturation condensation particle counter applied as a nano-CCN counter for size-
645 resolved analysis of the hygroscopicity and chemical composition of nanoparticles, Atmos.
646 Meas. Tech., 8, 2161–2172, https://doi.org/10.5194/amt-8-2161-2015, 2015.
647 Wiedensohler, A., Cheng, Y. F., Nowak, A., Wehner, B., Achtert, P., Berghof, M., Birmili, W.,
648 Wu, Z. J., Hu, M., Zhu, T., Takegawa, N., Kita, K., Kondo, Y., Lou, S. R., Hofzumahaus, A.,
649 Holland, F., Wahner, A., Gunthe, S. S., Rose, D., Su, H., and Pöschl, U.: Rapid aerosol particle
650 growth and increase of cloud condensation nucleus activity by secondary aerosol formation
651 and condensation: A case study for regional air pollution in northeastern China, J. Geophys.
652 Res.–Atmos., 114, doi:10.1029/2008JD010884, 2009.
653 Wiedensohler, A., Lütkemeier, E., Feldpausch, M., & Helsper, C. (1986). Investigation of the
654 bipolar charge distribution at various gas conditions. J. Aerosol Sci., 17(3), 413–416.
655 https://doi.org/10.1016/0021-8502(86)90118-7.
656 Zhang, R.: Getting to the Critical Nucleus of Aerosol Formation, Science, 328, 1366-1367, 2010.
657 Zhang, R., Khalizov, A., Wang, L., Hu, M., and Xu, W.: Nucleation and Growth of Nanoparticles
658 in the Atmosphere, Chem. Re., 112, 1957-2011, 2012.
659 Zhang, R., Suh, I., Zhao, J., Zhang, D., Fortner, E. C., Tie, X., Molina, L. T., and Molina, M. J.:
660 Atmospheric New Particle Formation Enhanced by Organic Acids, Science, 304, 1487-1490,
661 2004.
662 Zamora, I., Tabazadeh, A., Golden, D., and Jacobson, M.: Hygroscopic growth of common organic
663 aerosol solutes, including humic substances, as derived from water activity measurements,
664 Journal of Geophysical Research (Atmospheres), 116, 23207, 10.1029/2011JD016067, 2011.

Zieger, P., Fierz-Schmidhauser, R., Weingartner, E., and Baltensperger, U.: Effects of relative humidity on aerosol light scattering: results from different European sites, Atmos. Chem. Phys., 13, 10609–10631, https://doi.org/10.5194/acp-13-10609-2013, 2013.

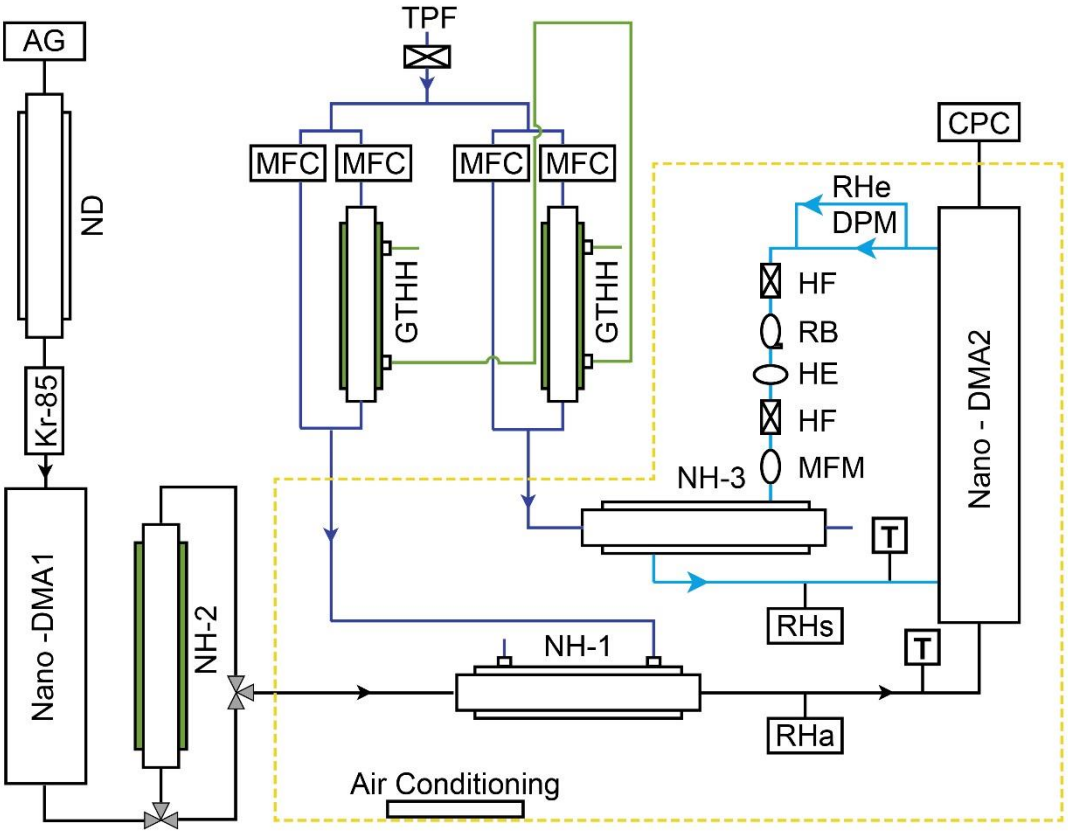

680

681 **Figure 1.** Experimental setup of the nano-HTDMA. Here, AG: aerosol generator (aerosol atomizer or electrospray);
682 ND: nafion dryer; Kr-85: Krypton source aerosol neutralizer; Nano-DMA: nano differential mobility analyzer; TPF:
683 total particle filter; HF: hydrophobic filter; MFC: mass flow controller; MFM: mass flow meter; RB: recirculation
684 blower; DPM: dew point mirror; GTHH: Gore-Tex humidifier and heater; NH: nafion humidifier; HE: heat exchanger;
685 CPC: condensation particle counter; Black line: aerosol line; Blue line: sheath line; Royal blue line: humidified air;
686 Green line: MilliQ water (resistivity of 18.2 MΩ cm at 298.15 K). RH_a and RH_s (measured by RH sensors) represent
687 the RH of aerosol and sheath flow in the inlet of nano-DMA2, respectively. RH_e (measured by dew point) represents
688 the RH of excess air. T represent the temperature of aerosol and sheath flow in the inlet of nano-DMA2, respectively.

689

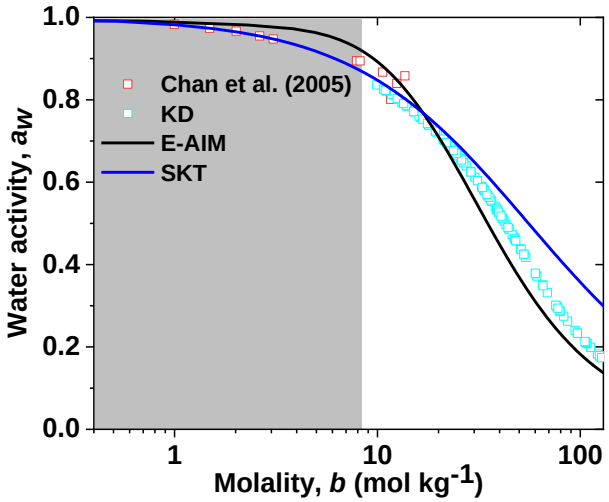

Figure 2. Concentration-dependent water activity (a_w) of levoglucosan solution. The KD-derived a_w (KD=Kreidenweis, cyan open square) is compared with observations (red open square), E-AIM (Extend-Aerosol Inorganic Model, black line), and a_w model (SKT, blue line). The light grey shaded areas mark the sub-saturated concentration with respect to bulk solution.

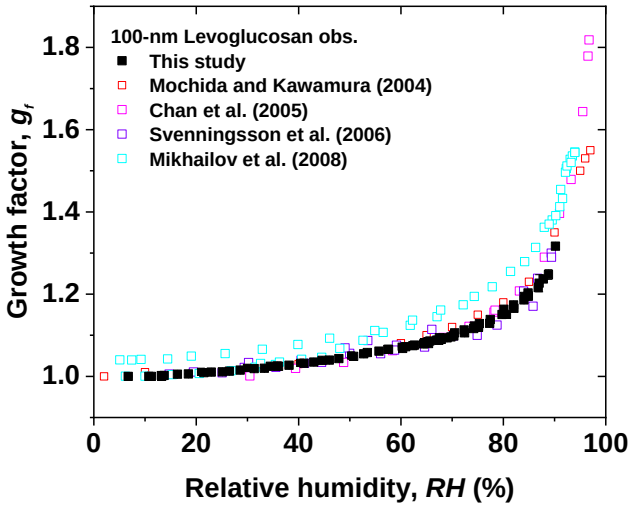

710

711 **Figure 3.** Hygroscopic diameter growth factor (G_f) of levoglucosan particles with dry diameter of 100 nm in both
712 deliquescence and efflorescence mode processes (black solid square). The measured data compared with literature data
713 from Mochida and Kawmura (2004) in both deliquescence and efflorescence modes (red open square), Chan et al.
714 (2005) in the deliquescence mode (magenta open square), Svenningsson et al. (2006) in the deliquescence mode (violet
715 open square), and Mikhailov et al. (2008) in both deliquescence and efflorescence modes (cyan open square).

716

717

718

719

720

721

722

723

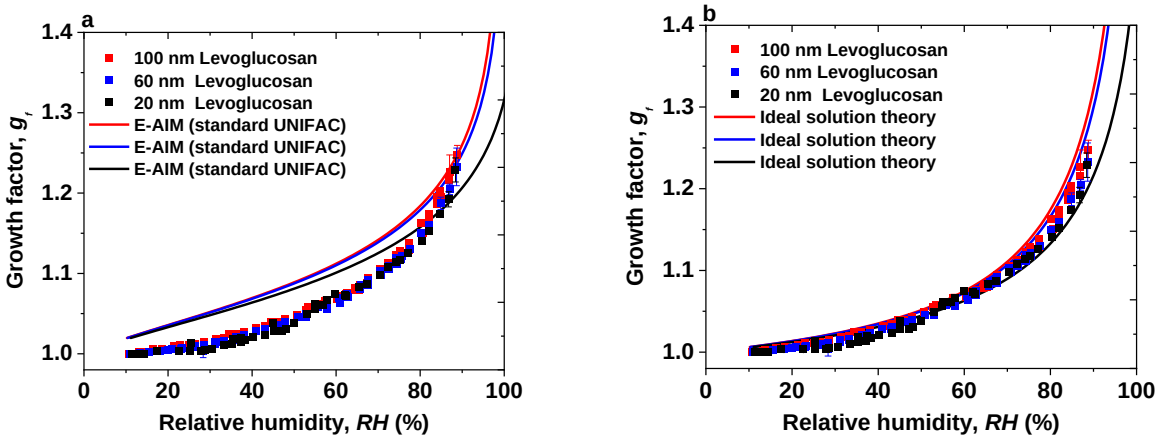

Figure 4. Hygroscopic diameter growth factor (G_f) of levoglucosan particles with dry diameter of 100 nm (red square), 60 nm (blue square), and 20nm (green square). Köhler model curves are based on: **(a)** E-AIM (standard UNIFAC) (100 nm: red, 60 nm: blue, 20 nm: green line), **(b)** ideal solution theory (100 nm: red, 60 nm: blue, 20 nm: green line).

739

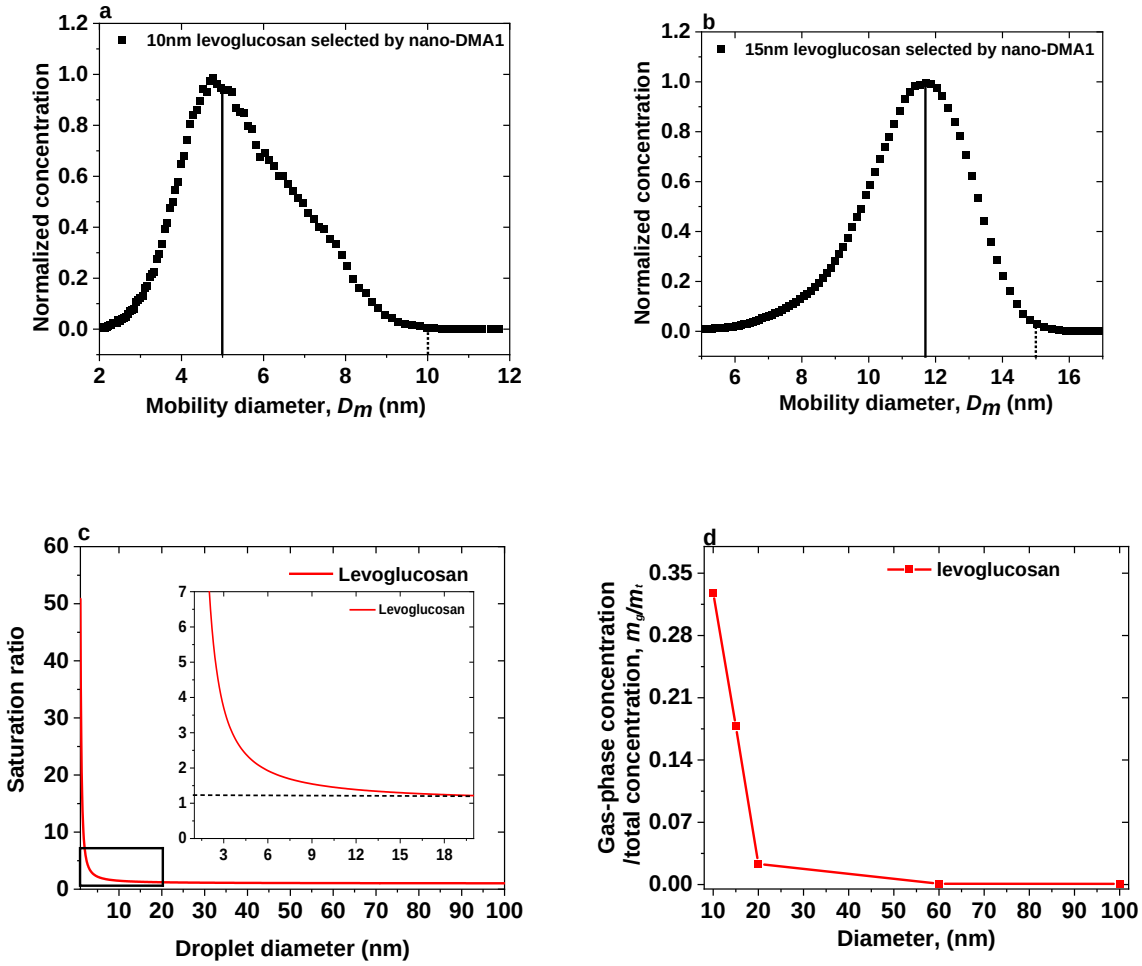

740

741 **Figure 5.** The normalized size distributions scanned by nano-DMA2 for: **(a)** 10 nm and **(b)** 15-nm levoglucosan at 10%
742 at 298K. The dotted lines mark the diameters of the monodispersed nanoparticles selected by the nano-DMA1. The
743 back solid lines mark the peak diameters from the normalized size distributions scanned by the nano-DMA2. **(c)** Vapor
744 saturation ratio of levoglucosan as a function of nanodroplet diameter according to the Kelvin equation. The diameter
745 range 1-20 nm for the saturation ratio of levoglucosan particles is shown as an inset. The value of surface tension of
746 pure levoglucosan is 0.0227104 [J m^{-2}]. **(d)** The ratio of gas-phase concentration (m_g) to the total concentration (m_t) of
747 levoglucosan nanoparticles against diameter.

748

749

750

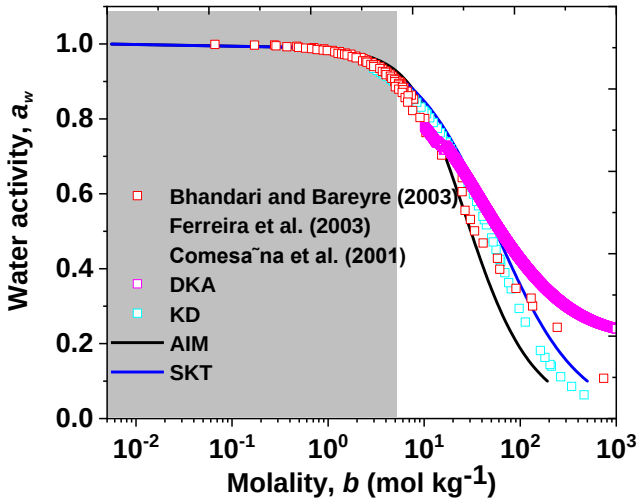

751

752 **Figure 6**. Concentration-dependent water activity (a_w) of D-glucose solution. The DKA-derived a_w (Differential

753 Köhler Analysis, magenta open square) is compared with observations (red open square), E-AIM (Extend-Aerosol

754 Inorganic Model, black line), a_w model (SKT, blue line), and parameterization model for a_w (KD=Kreidenweis, cyan

755 open square). The light grey shaded areas mark the sub-saturated concentration with respect to bulk solution.

756

757

758

759

760

761

762

763

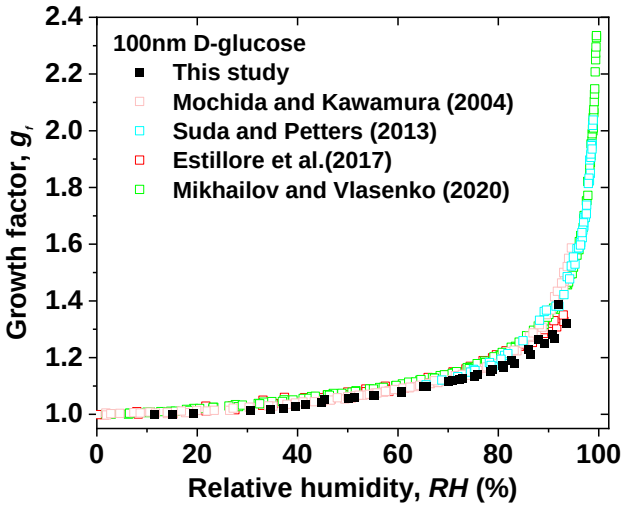

764

765 **Figure 7.** Hygroscopic diameter growth factor (G_f) of D-glucose particles with dry diameter of 100 nm in both
766 deliquescence and efflorescence modes (black solid square). The measured data compared with reference data from
767 Mochida and Kawmura (2004) in both deliquescence and efflorescence modes (pink open square), Suda and Petters,
768 (20017) in deliquescence mode (violet open square), Estillore et al., (2017) in both deliquescence and efflorescence
769 modes (red open square), and Mikhailov and Vlasenko (2020) in both deliquescence and efflorescence modes (green
770 open square).

771

772

773

774

775

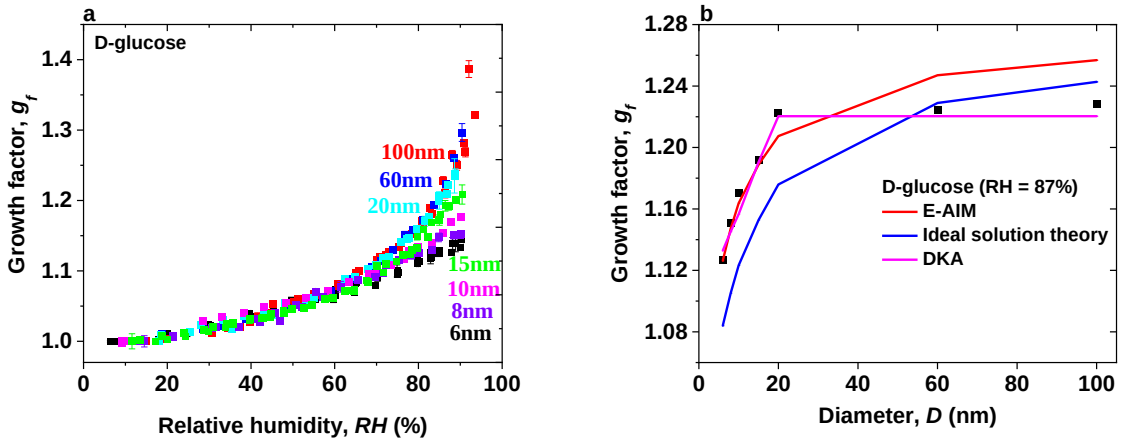

Figure 8. (a) Hygroscopic diameter growth factor (G_f) of D-glucose nanoparticles with dry diameters of 100 nm (red square), 60 nm (blue square), 20 nm (cyan square), 15 nm (green square), 10 nm (pink square), 8 nm (royal square), and 6 nm (black square). **(b)** Hygroscopic diameter growth factor (G_f, black square) of D-glucose nanoparticles with dry diameters from 6 to 100 nm at 87% RH. The measured hygroscopic growth factors of D-glucose nanoparticles with diameters from 100 down to are compared with E-AIM model (red line), ideal solution theory (blue line), and DKA prediction (pink line).

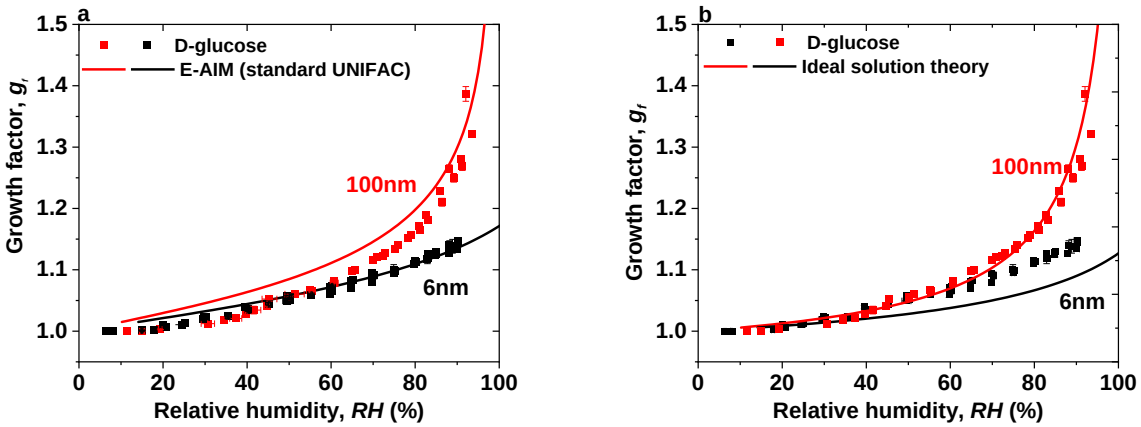

789

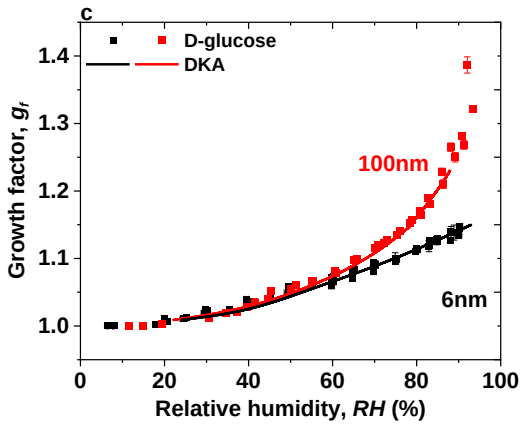

790

791 **Figure 9.** Hygroscopic diameter growth factor (G_f) of D-glucose nanoparticles with dry diameters of 100 nm (red
792 square) and 6 nm (black square). Köhler model curves are based on: **(a)** AIM (standard UNIFAC), (100 nm: red, 6 nm:
793 black line), **(b)** ideal solution theory (100 nm: red, 6 nm: black line), and **(c)** DKA mode (100 nm: red, 6 nm: black
794 line).